scientific reports

Check for updates

OPEN

Bifidobacterium adolescentis is resistant to pyrazinamide, isoniazid, and streptomycin

Anagha Nellikka[1,3], Athira Cheruvari[1,3], Prasanna Vasu[2,3], Sarma Mutturi[3,4] & Kammara Rajagopal[1,3]✉

The current study aims to understand the resistance of *Bifidobacterium adolescentis* to different anti-tubercular drugs (first-line oral tuberculosis drugs). The bacteria were grown with anti-tubercular drugs such as isoniazid, pyrazinamide, and streptomycin to better understand the resistance phenomena. It was found that even at tenfold higher concentrations, growth rates remained unchanged. In addition, a small number of bacteria were found to aggregate strongly, a property that protects against the toxicity of the drug. Further FE-SEM (Field Emission Scanning Electron Microscopy) analysis revealed that some bacteria became excessively long, elongated, and protruded on the surface. Size scattering analysis confirmed the presence of bifidobacteria in the size range of 1.0–100 µm. After whole genome sequence analysis, certain mutations were found in the relevant gene. In vitro, foam formation and growth in the presence of H_2O_2 and HPLC (High Performance Liquid Chromatography) studies provide additional evidence for the presence of catalase. According to RAST (Rapid Annotation Using Subsystems Technology) annotation and CARD (Comprehensive Antibiotic Resistance Database analysis), there were not many components in the genome that were resistant to antibiotics. Whole genome sequence (WGS) analysis does not show the presence of bacteriocins and antibiotic resistance genes, but few hypothetical proteins were observed. 3D structure and docking studies suggest their interaction with specific ligands.

Keywords Anti-tubercular drugs, MDR-*Mtb*, Bifidobacteria, *rpsl*

An important global problem is the high incidence of *Mycobacterium tuberculosis* (Mtb) infections that lead to tuberculosis. Most people with tuberculosis do not show any symptoms, but are nevertheless the main problem, as they contribute significantly to the spread of the disease according to the World Health Organization (WHO)[1]. Effective anti-tuberculosis drugs are readily available, but improper and excessive use has become a major problem. Strict adherence to the recommended three-month dosage is essential to prevent the development of new drug-resistant strains of mycobacteria, including totally drug-resistant (TDR), extensively drug-resistant (XDR) and multidrug-resistant (MDR) strains. The necessary genes, such as *rrs*, *rpsL* and *rpoB*, are mutated to produce these resistances. Researchers have studied and published specific (genetic, and phenotypic) changes in different species that lead to resistance to different drugs. Yuling Wang et al. (2019) have reported specific mutations that correlate with streptomycin resistance in *Mtb*[2] in 16s rRNA, *rpsL*, *rrs* and *gidB*. The *katG*, *inhA* and *aphC* genes of *Mycobacterium tuberculosis* were confirmed by first-time genome-wide alterations reported by P. Kiepela et al. (2000)[3] in INH-treated cells. Pyrazinamide (PYR) resistance and associated genes of *Mtb*[4] were linked to pyrazinamidase (*pncA*, *rpsA*) for the first time, according to Aditi Singh et al.. Rifamycin (*rpoB*, *rrs*), ethambutol (embB) and kanamycin resistance have also been discovered and reported; some studies have been conducted based on these genes[5–8]. Another gene, *rrs* encodes the 16 S rRNA; the most common, very frequently observed mutations are in loop 530 and region 912[9]. Identical mutations in some housekeeping and affected genes have even been observed in the drug-resistant Bifidobacteria spp. Here, *Mtb* is a lethal and chronic pathogen with resistance to anti-tuberculous drugs; now, extensive use of these drugs or horizontal gene transfer may have induced anti-tuberculous drug resistance even in bifidobacteria.

[1]Department of Biochemistry, CSIR- Central Food Technological Research Institute (CFTRI), Mysuru, Karnataka570020, India. [2]Department of Food safety and Analytical Quality Control Laboratory, CSIR- Central Food Technological Research Institute (CFTRI), Mysuru, Karnataka570020, India. [3]Academy of Scientific and Innovative Research (AcSIR), Ghaziabad201002, India. [4] Department of Microbiology and Fermentation Technology, Central Food Technological Research Institute (CFTRI), Karnataka 570020 Mysuru, India. ✉email: rajagopalk@cftri.res.in

The most effective broad-spectrum antibiotics currently available for the treatment of MDR-*Mtb*, XDR, and TDR are rifampicin (RIF), pyrazinamide (PYR), isoniazid (INH) and streptomycin (SM). These anti-tubercular drugs are considered highly effective for the treatment of chronic diseases such as tuberculosis (TB) and brucellosis[10–12]. Previous studies have shown that the addition of RIF to a culture medium changes the shape of the cells so that they no longer appear smooth but "rough"[13]. Brucella with a rough surface is less virulent and resistant to RIF than bacteria that are susceptible to RIF, which has potential implications for vaccination against brucellosis[14]. The β-subunit gene of RNA polymerase (*rpoB*) has been extensively studied to understand the genetic basis of RIF resistance in various prokaryotes and pathogenic microbes, including *Mtb*. Researchers have found that specific mutations in this gene cause rifampicin resistance and also impair glutamine metabolism[15].

In our previous study, we found that *B. adolescentis* is inherently resistant to the anti-tubercular drug RIF[16]. However, there are few studies explaining PZA resistance and the mechanism: PZA is a pro-drug that diffuses into the cytoplasm of *Mtb*. The enzyme pyrazinamidase (*PncA*) hydrolyzes PZA to pyrazinoic acid (POA)[17]. POA accumulates in the cytoplasm and initiates an entry exit cycle that releases protons and damages the cell by collapsing the membrane[18]. This is a type of permeabilization of the cell wall[19]. Several theories have been proposed about its mode of action, but most of them have been rejected[20,21]. Pyrazinamidase is a member of the class of isochorismatase (CATH) enzymes. The isochorismatase enzyme (GenBank: EDN83202.1) was discovered in *B. adolescentis*, but its functions differ from those of other species. Whole genome sequencing (WGS) studies have revealed that Bifidobacteria can catabolize POA in different ways. *PncA* Acc No. CUN64166.1 is present in *B. adolescentis*, although the corresponding gene has not yet been identified. Isoniazid, a pro-drug that requires catalysis of the enzyme catalase for activation, is another very effective drug. Catalase, which targets *inhA* and helps in the production of fatty acids, converts isoniazid into isonicotinic acid in the cytoplasm of the *Mycobacterium*. This prevents the formation of mycolic acid, which leads to cell death[22]. Therefore, if there is a mutation in the responsible gene, *KatG*, INH resistance develops. Recent studies have shown that *B. adolescentis* is a microaerophilic bacterium that does not possess a catalase[23]. This is the first case in which resistance of *B. adolescentis* to certain antitubercular drugs such as PYR and INH has been demonstrated.

The study isolated and identified *B. adolescentis* with *rpsL* mutations associated with the tuberculosis-resistant phenotype. The process begins with the bacteria growing in the presence of PYR, SM and INH. The relevant genes, *rpsL*, *rrs* (16 sr RNA gene) and *gidB* in the case of the SM-treated bacteria, were then amplified by PCR on the resulting bacteria. The isochorismatase nicotinamidase PYR is a homolog of the pyrazinamidase of *Mtb*. To detect changes in INH-treated bacteria, the corresponding catalase genes were analysed in whole genome sequencing (WGS), amplified and sequenced. The results were then compared with MDR, XDR[24] and TDR-*Mtb* genes. According to current reports and the WGS study, *B. adolescentis* does not contain catalase. However, our biochemical and preliminary studies show that catalase is present. Since bifidobacteria are resistant to anti-tubercular drugs, they can be used in probiotic and antibiotic treatment[25]. The main objective of the study is therefore to understand the mechanistic and morphological aspects of anti-tubercular drug resistance in *B. adolescentis*.

Results

Growth curve studies and analysis

In our study, PYR, INH and SM were administered to understand resistance to tuberculosis in *B. adolescentis*. Since PYR dissolves in (5.0%) Dimethyl sulfoxide (DMSO), cells were cultured in DMSO, De Man–Rogosa–Sharpe (MRS) alone and MRS in combination with PYR. It is known that PYR is only activated at low pH (5.8). At low pH (< 6.0), we observed in the present study that *B. adolescentis* grew to an OD_{600} of 3.0; normally it takes 36 h to reach an OD_{600} of 3.5. It was found that the cells treated with PYR (1.0 mg/mL) grew very slowly and never exceeded an OD_{600} of 1.5. The stationary phase was achieved by very short log and lag phases and maintained over a prolonged period (Fig. 1A). Similarly, the Bifidobacteria cells treated with 3.5% ethanol were used as controls in the FE-SEM analyses performed on the INH-exposed cells. As expected, the control group showed normal growth, but the INH (1.0 mg/mL) treated group did not develop beyond 3.0 OD_{600}. At 36, 42 and 54 h, there were some zigzag growth trends until the group finally reached the stationary phase (Fig. 1B). Another antitubercular drug commonly used for treatment is streptomycin, which has very high efficacy against *Mtb*. The analyses of the growth curves were performed considering the different ranges of SM. The growth rates of 25–100 µg/mL SM-treated bifidobacteria were analysed. We found that the lag phase increased and the log phase decreased with increasing SM concentration. The results clearly show that only cells treated with 25 µg/mL SM could reach an OD_{600} of 3.0. However, the cells treated with 50–100 µg/mL were not able to achieve an OD_{600} of more than 2.0. The cells treated with 100 µg/mL were only able to achieve an OD_{600} of 0.8 (Fig. 1C). These results are convincing evidence that higher concentrations can significantly impair the growth rate. Due to the slow growth, it took about 60 h for the OD_{600} to reach 0.8. To better understand the actual viability at higher growth concentrations, we conducted sampling studies to gain a clearer understanding of the results.

Spot assay to understand viability after treatment with various anti-tubercular drugs

Fresh MRS medium was used to culture *B. adolescentis* for 72 h at 37 °C under anaerobic conditions without shaking. They were then serially diluted to 10^{-1}–10^{-5}. 1 µL of each dilution was then spotted onto several anti-tuberculous drug-containing plates, including those containing SM, INH, and PYR. The ethanol, DMSO and system controls were all plated in a similar manner. Cells treated with 1.0 mg/mL INH showed signs of viability; this was the case even at the lowest amount. However, viability was the same in the ethanol-treated sample as in the control. The SM-treated cells showed much lower viability, with almost no viable cells detected at dilutions of 10^{-4} and 10^{-5}. The results were similar for the PYR-treated bifidobacteria. The concentrations studied were about five times higher than those for MDR, XDR and TDR-*Mtb*. The bifidobacteria were able to grow and multiply even at such high concentrations, and their viability was observed. More specifically, the bifidobacteria

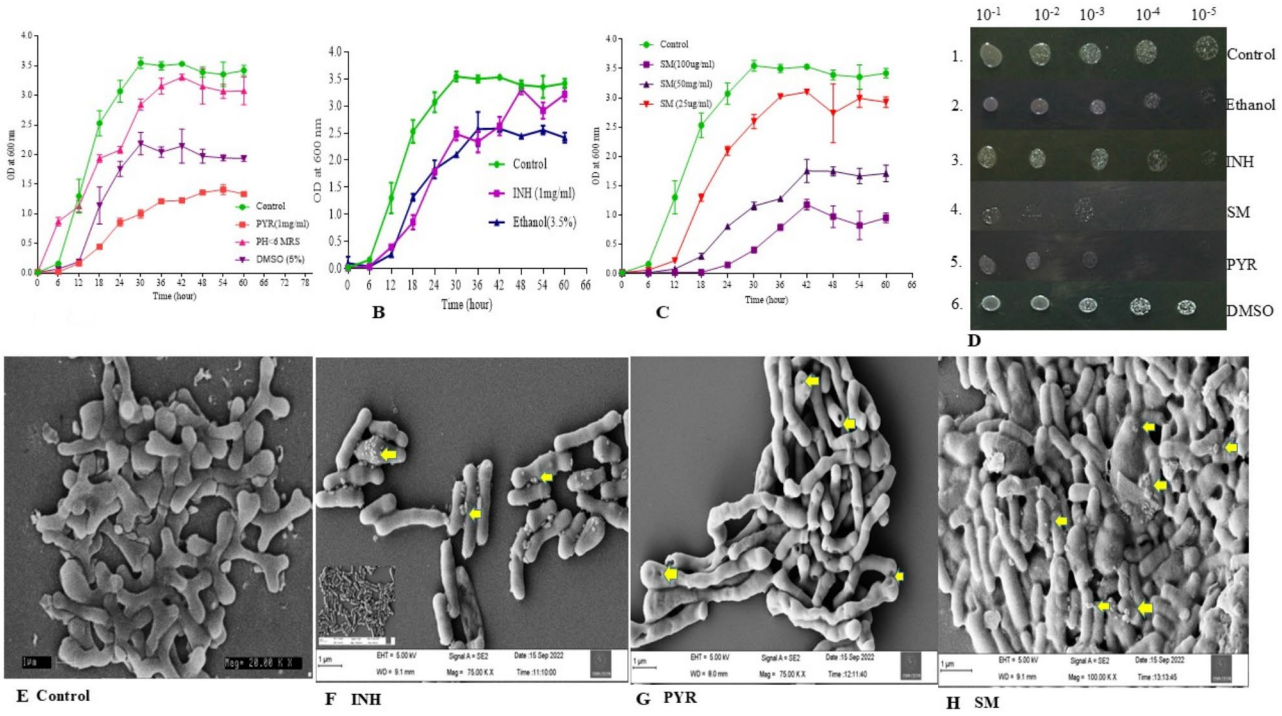

Fig. 1. (**A**–**C**) represent growth curves of *B. adolescentis* in presence of anti-tubercular drugs such as PYR (**A**), INH (**B**), and SM (**C**). The procedure followed in brief; streaked, isolated single colony was grown in fresh 10 mL MRS broth. Grown at 37 °C for 72 h, later 1.0% was inoculated into 100 mL fresh MRS broth. The initial OD_{600} kept at 0.0.01, and growth was continued, after every 6 hour interval samples were collected and OD_{600} was measured. Finally, after 60 h graph was plotted between OD and Time. The experiment was performed thrice and average was taken. (**D**) Spot assay. 72 h grown Bifidobacterial cultures were diluted 10^{-1}–10^{-5} subsequently, 1 µl of these cultures were spotted on various anti-tubercular drug containing plates. The growth was observed by incubating them at normal growth conditions. (**E**–**H**) The Bifidobacteria grown in the presence of various anti-tubercular drugs were withdrawn after 72 h and harvested the cells by centrifugation at 5000 rpm for 10 min. Cells were washed with phosphate buffer, subsequently, fixed with glutaraldehyde and incubated at 4.0 °C overnight. Later the cells were washed with 10–100% ethanol gradient. Finally re-suspended in absolute alcohol (50–100 µL), an aliquot (~ 2.0 µL) of the sample was placed on a cover slip, desiccated and observed using FE-SEM. (**E**) Represents control Bifidobacteria (Simple SEM picture), (**F**) indicates INH treated cells, yellow arrow indicates protrusions on the surface, (**G**) represents-PYR treated cells yellow arrow indicates holes on the surface and the terminal, and (**H**) represents SM treated cells yellow arrow indicates the presence of surface protrusions.

grew at concentrations ten times higher than MDR-*Mtb*, although the latter could only tolerate 100 µg/mL SM. Bifidobacteria thus have the ability to adapt to various harsh conditions (Fig. 1D). Figure 1E shows the control *B. adolescentis* followed by the Bifidobacteria treated with INH (Fig. 1F), Fig. 1G shows the *B. adolescentis* treated with PYR followed by the *B. adolescentis* treated with SM.

MIC determination

The MICs of *B. adolescentis* for PYR, INH and SM are listed in Table 1, together with the reported MICs of MDR, XDR and TDR-*Mtb*. According to Keira et al. (2020), *Mtb* has an MIC of 0.5–1.0 µg/mL. The MIC shifts to 2.0 µg/mL for the *gidB* mutation, 32 µg/mL for the *rpsL* mutation and 32 µg/mL for the *rrs* mutation when it mutates. We have shown for the first time that *B. adolescentis* is resistant up to 100 µg/mL of SM (streptomycin), which corresponds to a hundredfold increase. The minimum inhibitory concentration (MIC) of MDR-*Mtb* for isoniazid (INH) is 0.0312 µg/mL, while for pyrazinamide (PYR) it is 50 µg/mL. Bifidobacteria have the highest MIC for PYR at 500 µg/mL and for INH at 1000.0 µg/mL. The results clearly show that *Bifidobacterium* is highly resistant to anti-tubercular drugs compared to MDR/XDR *Mtb* (Table 1).

Field emission scanning electron microscopy studies (FE-SEM)

The following results are expected from FE-SEM studies of *B. adolescentis* treated with INH anti-tubercular drugs: Fig. 1E shows a control sample of bifidobacteria, while Fig. 1F shows abnormal cells with surface protrusions; aggregation is a typical phenomenon. Most significantly, no cells with the shape of a bifid were seen. Smoothness, mere rod shape, protrusions or external growth, aggregation and even damaged cells are characteristics of normal cells. In Fig. 1E–H, arrows indicate external growth or surface protrusions. The structure of bifidobacteria is shown in the inset figure. Since INH is dissolved in ethanol, this serves as a control.

S. No	AntiTB Drug	Wt	MIC MDR/XDR µg/ mL	Bifidobacteria (µg/mL)	Reference
1	Sm	0.5-1.0	2.0 *gid* B mutn	100	https://doi.org/10.1128/AAC.00860-20
			32 *rpsl*		
			32 *rrs*		
2	INH		0.0312	1000.0	http://doi:https://doi.org/10.1093/cid/ciy346
3	PYR		50	500	

Table 1. MIC of *Mtb* and Bifidobacteria (and variants). The MIC of *Mtb* was of previous reported and the references were also enclosed. The MIC obtained in the case of Bifidobacteria were obtained in the present experiments by following broth dilution assay. SI No.1 corresponds to Sm treated Bifidobacteria and their MIC, followed by INH at SI No.2, and PYR MIC at SI No.3. MIC of MDR/XDR *Mtb* are shown.

FE-SEM studies were also performed on bifidobacteria treated with PYR. The cells treated with DMSO alone were analysed by FE-SEM and showed normal morphology with no changes (Fig. 1G). However, the cells treated with PYR (which is dissolved in DMSO at a concentration of 1.3%) showed a loss of bifid shape, with the terminal ends exhibiting hollow, roundish holes. Although observed at the surface, cell aggregation was also observed. Further abnormal elongation, indicating loss of cell division, and a rough cell surface were the most common observations (Fig. 1G). After dissolving SM in sterile MQ water, the other anti-tuberculous drug was analysed by FE-SEM. Similar to the previous findings, we discovered that the cells had lost their bifid shape, which is very common; instead, they were short, enlarged and clumped. The fact that a thread-like mucus is now visible between the cells—something that was not observed in previous treatments—is a really interesting finding. Here it was observed that all cell surfaces are rough (Fig. 1E–H).

Particle size analyzer

To determine the size of the bacterial cells, the bifidobacteria were exposed to different doses of anti-tuberculosis drugs and then analyzed using a particle size analyser. The cells in the control group had a diameter of 2.49 µm and 2.32 µm, with 53.4% of the cells having these typical dimensions. However, the SM-treated cells had significantly larger diameters and width compared to the other cells. Even the diameter and width of the PYR-treated cells were at the upper end. In 68% of the cells treated with 100 µg/mL SM, a very high diameter of 25.08 µm and a width of 40.18 µm were observed. No significant change was observed with the other concentrations and additional anti-tuberculous drugs (Fig. 2A–F).

Mutations and their detection

Numerous drugs have been used to treat bifidobacteria under various conditions. Their gDNA was extracted as previously described. The corresponding genes, including *gidB*, *rrs* and ribosomal S12 protein (*rpsL*), were amplified and their DNA sequenced. The explanation is that these mutations conferring resistance have been shown to be present in MDR, XDR and TDR-*Mtb*. On this basis, we performed the same study with bifidobacteria (Fig. 2G). No mutations were found. However, a mutation in the *rpsL* gene at the 88th amino acid residue was only found in the samples treated with 150 µg/mL SM. No effect was observed at 25 and 50 µg/mL SM (Fig. 2G). The arrow in the figure shows the nucleotide change from A to G, turning AAG into AGG, which corresponds to arginine; no other mutations were observed.

Foam assay to detect the catalase

The enzyme catalase catalyzes the conversion of inactive isoniazid into active isonicotinic acid. Activated isonicotinic acid further acts on isoniazidase, which is involved in the synthesis of mycolic acid/fatty acid in *Mycobacterium tuberculosis*. Catalysis of the enzyme catalase leads to the inhibition of isoniazidase, which is the mechanism and mode of action of INH. The resulting isoniazidase inhibits cell wall synthesis. Therefore, it is used as an anti-tuberculous drug. Therefore, we need to determine whether the host contains catalase. For this purpose, the simple visible foam test was followed. The cells were grown under three different conditions: aerobic (4.0 mL culture in a 15 mL Falcon tube, live and with more oxygen content); and microaerophilic (12 mL culture in a 15 mL Falcon tube). In addition, cells were grown in a 15 mL flask without aeration. Samples were taken at six-hour intervals. The cells were then harvested, washed and tested with the foam assay. The results clearly show that foam formation increases with increasing growth rate. Initially, no foam appeared; only when the bacteria were cultured in a microaerophilic environment was there clearly visible foam. No foam was visible under both anaerobic and purely aerobic conditions (Fig. 2H,I). The foam that was visible remained constant and did not dissolve.

Zymogram for on gel catalase detection

The basic method for measuring catalase activity involves the reaction of ferric chloride and potassium ferricyanide (III) in the presence of hydrogen peroxide. In the case of recombinant catalase from *B. asteroids*, a distinct achromatic band was seen against a green-blue background; the intensity of the band was extremely high. A similar band was also seen in the *B. adolescentis* samples, but it was much less intense. Removing and transferring the gel to MQ water helped to eliminate the overstaining (Fig. 2I inset, lane 1: *B. asteroids* Rec. catalase, lane 2: *B. adolescentis* catalase).

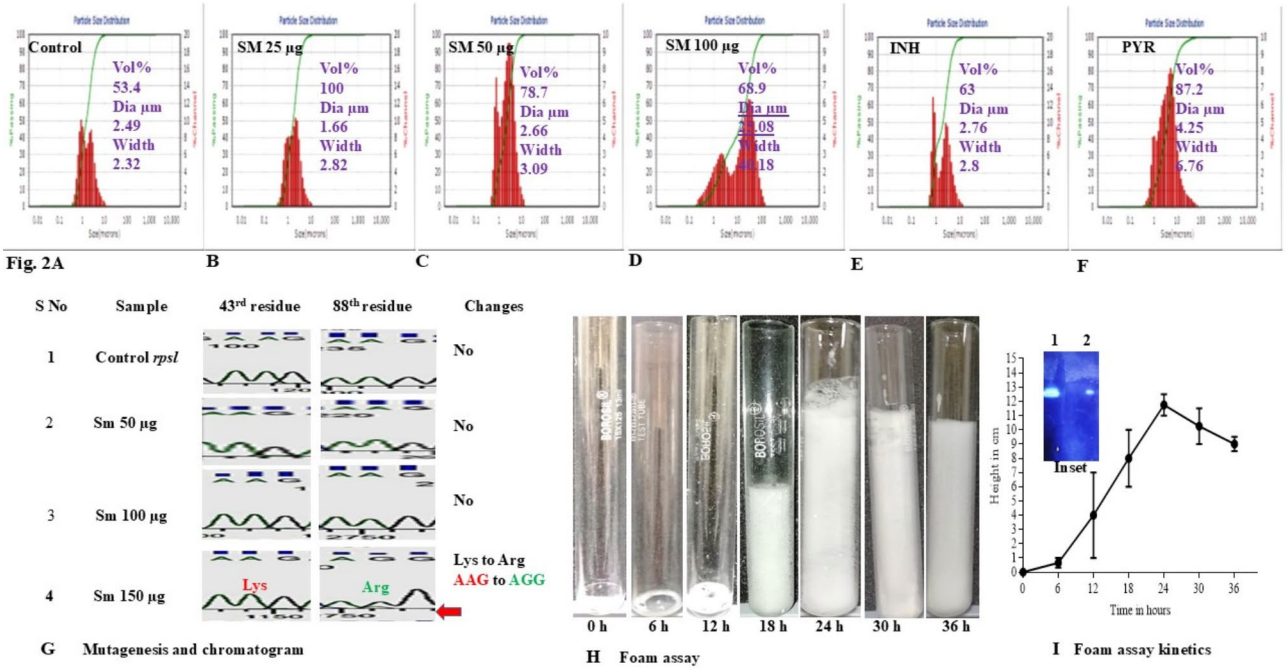

Fig. 2. (**A–F**) Represents the volume, diameter and width of *B. adolescentis* treated with anti-tubercular drugs. Cells grown as explained above were washed with sterile MQ water twice and then subjected to particle size analyser system. The final results were analysed and shown in the figure. (**G**) Bifidobacteria were grown in the presence of anti-tubercular drugs of various concentrations. They were harvested and washed with sterile phosphate buffer. gDNA was purified and subjected to Sanger DNA sequencing. Although we sequenced many genes, but we found mutations with certain genes that are presented. Final focus was kept on *rpsl* 43rd and 88th amino acid residue. As these considered to be hot-spots and conserved even in MDR-*Mtb*, XDR, and TDR these are the residues with amino acid variations observed. Therefore, the sequence of samples is (1) Control Bifidobacteria, (2) *B. adolescentis* treated with 50 µg of Sm, followed by 100 µg, and 150 µg. The red arrow in the lane 4 indicates Lys to Arg mutation the same thing has been shown in the chromatogram. At the end the changes were mentioned, most of the cases no changes were observed, and only at highest concentration of Sm the change has been mentioned. (**H**) Foam assay. Tadayuki Iwase et al., 2013 method was followed it is a simple assay used to measure catalase activity. In brief, the Bifidobacteria were inoculated in 100 mL of fresh MRS media, grown as discussed above. The samples were collected at various intervals such as 0, 6, 12, 18, 24, 30, and 36 h harvested, washed with phosphate buffer and pellet was directly used or even dissolved in very small quantities of sterile Tris.cl buffer or phosphate buffer. Subsequently, 100 µL of Triton-X-100, followed by 100 µL of H_2O_2 were added, mixed and incubated at room temperature. Fig I represent foam assay kinetics. Foam assay kinetics shows height of the foam formed at various timest (0, 6, , 12, , 18, 24, , 30, and 36 h). (**I**, **Inset**). Inset shows the active catalase, the Magdalena Pezzoni et al. 2018 procedure was followed. The procedure in brief; The native gels were electrophoretic separated, washed in MQ for ten minutes, incubated in a solution of freshly prepared 0.01% OR 4.0 mM H_2O_2 (made from a 30% stock) for ten minutes, and then rinsed in 100 mL of MQ for thirty minutes. The gels were then incubated in a freshly prepared solution containing 1.0% ferric chloride hexahydrate and 1.0% potassium ferricyanide trihydrate while being gently agitated. The gels were exposed as per the requirement of the intensity of the protein bands.

Anti-tubercular drug uptake and surface analysis

Figure 3A–C show the High-Performance Liquid Chromatography (HPLC)-based estimation of the uptake of anti-tubercular drugs by the bacterium. Figure 3B, C show remarkable differences in the HPLC pattern indicating the uptake and subsequent conversion of INH in Fig. 3B and PYR in Fig. 3C. This clearly demonstrates the ability of *B. adolescentis* to take up and metabolize drugs. The control HPLC peaks are shown in the insets of Fig. 3. *B. adolescentis* treated with drugs shows aggregation on its surface accompanied by a yellow background. The surface of the bacterium was rough, which is characteristic of both the control and acrylamide-treated organisms. Figure 3B The image of the acriflavine staining clearly shows the uptake of the dye by the aggregated bacterium with a yellow background. The front row shows the controls of *B. adolescentis*, including the 1st lane treated with test bacteria, followed by INH, SM, low pH and PYR treated *B. adolescentis*.

Adaptability studies

Cell lysates were obtained by lysis of bifidobacteria cultured either in the presence or absence of various anti-tubercular drugs such as PYR and INH. After the sample were prepared for HPLC studies, they were subjected

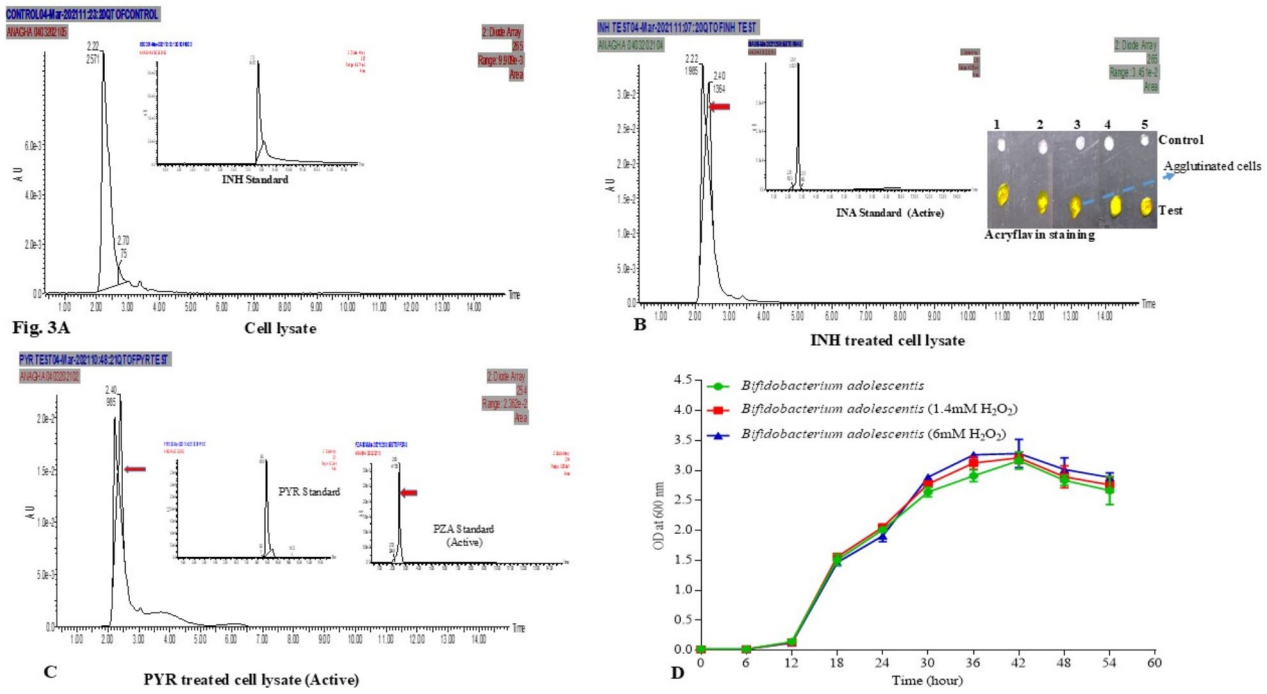

Fig. 3. Anti-tubercular Drug Uptake: Bifidobacterial cells were incubated with various anti-tubercular drugs such as INH, and PYR. The treated cells were harvested, washed, and lysed; lysate was subjected to HPLC. The same procedure was followed for control cells that are un-treated, and even standards such as INH, and PYR were also subjected to HPLC. As few drugs are dissolved in certain chemicals such as DMSO, and Ethanol. Therefore, they were also taken into consideration for HPLC. (**A**) Shows HPLC pattern of cell lysate, the inset shows INH standard, (**B**) Shows INA standard inset (activated compound), INH treated sample shows big HPLC peak. (**C**) PYR treated Bifidobacterial cell lysate, the inset showing PYR standard and PZA standard (active form). Inset: Shows acryflavin treated *B. adolescentis* to understand their cell surface smooth or rough. Once cells have been exposed to anti-tubercular drugs to understand their cell surface texture agglutination reaction with acryflavin solution (1/1000) and capacity to uptake crystal violet was followed. Brief procedure followed: A single isolated colony was chosen, and transferred onto the glass microscopic slide. Later, 10 µL of 0.1% acryflavin solution was added and incubated for five min at room temperature. Finally, image was captured for analysis. (**D**) Growth curve of Bifidobacteria in the presence and absence of different concentrations of H_2O_2. The growth curve of Bifidobacteria was followed with an initial OD_{600} of 0.01, in the presence of 1.40 and 6.0 mM of H_2O_2. At various intervals cells were taken to estimate its OD_{600}, the reaction was continued to 60 h. Finally, the graph was plotted between OD_{600} and time.

to HPLC. Compared to the control cell lysate (RT. 2.68, 15661), the peak area of the cell lysate from INH-treated cells was almost twice as high (RT. 2.68, 27160). Thus, INH-treated cell lysates, as determined by HPLC analysis at 265 nm–213 nm (using the DA detector), convert INH (Rt. 7.72) to another product, most likely active INA (RT. 2.40 or Rt. 2.68) (Fig. 3A, B-inset shows the INH standard, and B-inset represents the INA standard). Similarly, cells treated with PYR were converted to a different product, most likely active PZA (Rt. 2.40), as shown by HPLC analysis at 254 nm (using a DA detector). We assume that the RT of the typical active PZA (Rt. 2.50) varies but is the same, as the RT variation is less than 5.0%. The lysate, which absorbs at identical wavelengths, is responsible for the peak at 2.22 (Fig. 3C; one figure shows the PYR standard, the other the PZA standard).

Growth curve studies in the presence and absence of H2O2

Bifidobacteria have a slow growth rate with a doubling time of about 2.0 h. The cells treated with H_2O_2 remained in the lag phase for about 12 h. The presence of 6.0 mM H_2O_2 led to a decrease in the growth rate (in the initial phase). However, there was no significant effect of H_2O_2 (such as cell death); in fact, the 6.0 mM sample eventually grew faster than the control, indicating adaptation. The only difference observed was the prolonged lag phase when treated with H_2O_2. Figure 3D shows the growth curve of *B. adolescentis* with and without H_2O_2.

CARD, RAST analysis / antibiotic resistance gene identification

WGS (Whole genome Sequence Analysis) analysis, annotation was performed with the sequences. We wanted to find out the number of antibiotic-resistant genes and their localization. The antibiotic resistance genes (ARGs) of *B. adolescentis* were analysed using the Comprehensive Antibiotic Resistance Database (CARD)https://pubmed.ncbi.nlm.nih.gov/31665441/ 26. RAST annotation identified several antibiotic-resistant pathways in

B. adolescentis, such as copper homeostasis, bile hydrolysis, tetracycline- and fluoroquinolone-resistant and multidrug-resistant efflux pumps. CARD analysis revealed the presence of rifamycin and tetracycline resistance genes.

Cellular morphology studies

Bifidobacteria treated with various anti-tuberculous drugs were subjected to simple microscopic examination. The images were taken and it can be seen from Fig. 5A–D that the bacteria are very different from each other. This indicates that the bifidobacteria adapt their surface shape in order to survive. According to the results, the colonies showed a wide range of sizes and appearances, from tiny and translucent to large and milky white. Remarkably, the anti-tubercular-treated bacterial colonies showed more than two variants, while the control group showed only two different forms. All 4 colonies (untreated, SM-treated, INH-treated and PYR-treated) showed a crater-like (concave) shape. The untreated colony had a cloudy centre with a white, raised, round ring surrounded by a translucent, wavy rim (rough edge). Figure 5A Control *B. adolescentis* Fig. 5B (treated with SM) shows four different types of countable cell surfaces, including a cloudy colony with a slimy layer around it, as shown in the inset. These results indicate a significant effect of the anti-tubercular drugs on the diversity of bacterial colonies. Figure 5C shows three distinct regions: a milky white outer layer, a central cloudy zone and a white rim. Figure 5D shows two regions when the colony is treated with pyrazinamide: a translucent centre and a white rim that is not separated. The cell structure of the control cells and the INH-treated cells seems to be identical as they are white-milky. The only difference could be the rough edge in the case of the control, but the smooth edge in the case of the INH treatment.

3D-Structure prediction / docking

Using autodocking tools (1.5.7), the binding energy of the pyrazinamidase wild-type complex of *B. adolescentis* with PYR was − 4.26 kcal/mol. Some mutations ($^{S}102^{T}$ and $^{D}125^{N}$) were predicted based on the literature on *Mtb* resistance to PYR[27,28]. Their interaction with the ligand pyrazinamide was investigated. It was found that the complex of the expected mutation ($^{S}102^{T}$) binds much more strongly to the ligand than the wild type (binding energy: − 4.75 Kcal). However, compared to the wild type, mutant 2 ($^{D}125^{N}$) has a lower binding energy (− 3.81 kcal/mol). If the *Mtb* mutates to have a lower affinity for this enzyme (binding energy: − 3.81 kcal/mol), it is likely to develop resistance to PYR. Pyrazinamide-resistant strains have different gene mutations that are not transferable between strains. In a recent study, researchers found that the structure of the *Mtb* pyrazinamidase and the *rpsL* gene of DSM 20083 are not comparable. Nevertheless, the analysis focused on the mutant interaction between the *rpsL* gene and streptomycin, which was empirically demonstrated. The mutants showed stronger interactions with ligands than the wild type, as predicted by the binding energy values (− 1.27 kcal/mol for the mutants versus − 0.24 kcal/mol for the wild type) in this structure-binding prediction. This robust interaction between *rpsL* and streptomycin was observed in *B. adolescentis*, despite the resistance of the mutants (Fig. 6A–D).

Discussion

The study aims to understand why *Bifidobacterium adolescentis* is resistant to certain anti-tuberculosis drugs and how it adapts to them. Initial results indicate that growth is impaired with some drugs, while others significantly inhibit growth at higher concentrations. Previous studies on MDR, XDR and TDR-*Mtb* clearly conclude that the chronic disease-causing, globally infectious pathogens are resistant to no more than 1–50 µg/mL SM[26]. It is of great concern that the probiotic and highly beneficial microbe Bifidobacteria have resistance to very high concentrations of anti-tubercular drugs.

In the growth curve studies the lag phase lasted 24 h in cells treated with SM, regardless of the concentration (Fig. 1C). We started with a 10 µg/mL SM concentration for the present studies, but observed that the bifidobacteria adapted as we increased the SM concentration. Finally, no growth was seen at 150 µg/mL (Fig. 1C), a concentration about 100 times higher than the MDR *Mtb* MIC. This is concerning as bifidobacteria are generally recognized as safe (GRAS) organisms with probiotic properties. Other drug resistances in MDR, XDR, and TDR are at concentrations of 2–32 and 50 µg/mL, such as for INH and PYR. These results clearly indicate that bifidobacteria have resistance to tuberculosis and can adapt[29,30]. The MICs of antitubercular drugs are significantly higher in bifidobacteria than in drug-resistant *Mtb*. A spot assay showed that few viable cells were present when treated with certain drugs, prompting us to focus on WGS to identify the catalase gene responsible (Fig. 1D). After detailed investigation, it turned out that there is no catalase gene in *B. adolescentis* (no reports), but it was found in *B. asteroids*[31]. The preliminary biochemical studies in our laboratory show the presence of catalase in *B. adolescentis*.

Bifidobacteria treated with anti-tubercular drugs were examined using FE-SEM (Fig. 1E–H). INH-treated cells showed surface damage, while PYR and SM treatments led to abnormalities such as surface enlargement and hole formation (Fig. 1G,H). This might be a way for the cells to avoid drug toxicity by increasing surface area, potentially affecting drug uptake. We used a Microtrac particle size analyser to examine the size of bifidobacteria treated with anti-tubercular drugs. The treated bacteria differed in shape and size, especially in their width and diameter. Bifidobacteria treated with 100 and 150 µg/mL SM were 10 times wider and larger than others, suggesting that they could protect themselves by increasing their surface area. No significant differences in size were observed in bacteria treated with other anti-tubercular drugs (Fig. 2A–F).

Bifidobacteria treated with an anti-tubercular drug and corresponding resistant genes were subjected to DNA sequencing. Mutations were only observed in the *rpsL* gene at the 88th amino acid residue, with Lys changing to Arg in the samples treated with 150 µg/mL SM. No mutations were found at the 44th amino acid residue. This mutation was also observed in MDR-*Mtb*, confirming the rapid adaptability of *B. adolescentis* to drug resistance. No mutations occurred during treatment with PYR and INH. Nair et al. (1993) reported

exchangeable point mutations at codon 43 of the *rpsL* gene in clinical isolates and SmR-*Mtb rpsL* gene sequences. Identical mutations were found in SmR *E. coli*, indicating the presence of different resistance mechanisms[32]. Table 1 shows the MICs of the different *Mtb* and bifidobacteria.

Further genetic studies and biochemical investigations are required to understand the role of catalase in *B. adolescentis*. The foam test and growth observations indicate that *B. adolescentis* is a catalase-positive (Fig. 2H), microaerophilic organism closely related to *B. asteroides*. The experiments showed that foam formation increased with time, peaked after 24 h and then remained stable (Fig. 2H, I). This indicates the presence of catalase, which is necessary for survival in the presence of oxygen. The enzyme catalase converts INH into isonicotinic acid and thus inhibits the synthesis of mycolic acid, a common phenomenon in MDR-*Mtb*. Our studies on *B. adolescentis* show resistance, indicating the presence of catalase. A rapid test confirmed increased O^2 foam production, indicating catalase-positive bifidobacteria (Fig. 2H, I inset).

The bacteria were examined to see how they adapt to the anti-tubercular drugs. The studies showed that bifidobacteria can catalyze these drugs. One drug, PYR, was converted to PZA and another drug, INH, was converted to INA. Interestingly, the bacterium *B. longumLTBL16* lacks the genes for catalase or superoxide dismutase, yet it is able to tolerate oxygen and neutralize harmful substances[33]. The HPLC results confirmed that bacteria with the required enzymes can degrade these drugs.

We conducted growth analysis studies in varying H_2O_2 concentrations and observed no growth inhibition, demonstrating the presence of catalase and adaptability (Fig. 3D). Additionally, our HPLC studies showed drug uptake and transformation, with no morphological changes in the bacterial colonies post-uptake (Fig. 3A–C). The shiny, spherical surface of the colonies indicates potential higher pathogenicity compared to rough colonies. The genome of *B. adolescentis* was analyzed using RAST and CARD annotation data (Fig. 4A). This revealed 356 events related to protein metabolism, including resistance to several antibiotics (Fig. 4B). The results are shown in Fig. 4A-F.

In this study, *B. adolescentis* did not change colony morphology from rough (initial stage) to smooth after treatment with all three anti-tubercular drugs. The colonies of *B. adolescentis* are smooth, without abnormalities or roughness, they are white and round or circular. Colony 1 and colony 4 are different in size and their surfaces have a convex shape. Although the characteristics of colonies 2 and 3 are the same, their sizes vary. Some morphological changes were observed in the cells. For example, the isoniazid-treated cells have some colonies with the same characteristics as the control cells (Fig. 5A). Some colonies appeared as milky-white, smooth, round and shiny, with different sizes (See colonies 1,2 3 of Fig. 5B, C). After treatment with streptomycin, *B. adolescentis* showed three different cell morphologies. All colonies were translucent on the outside, whitish on the inside and had a smooth, shiny and round appearance. Pyrazinamide-treated *B. adolescentis* showed some variations in colony morphology, including smooth, shiny, convex and concave surfaces (Fig. 5D).

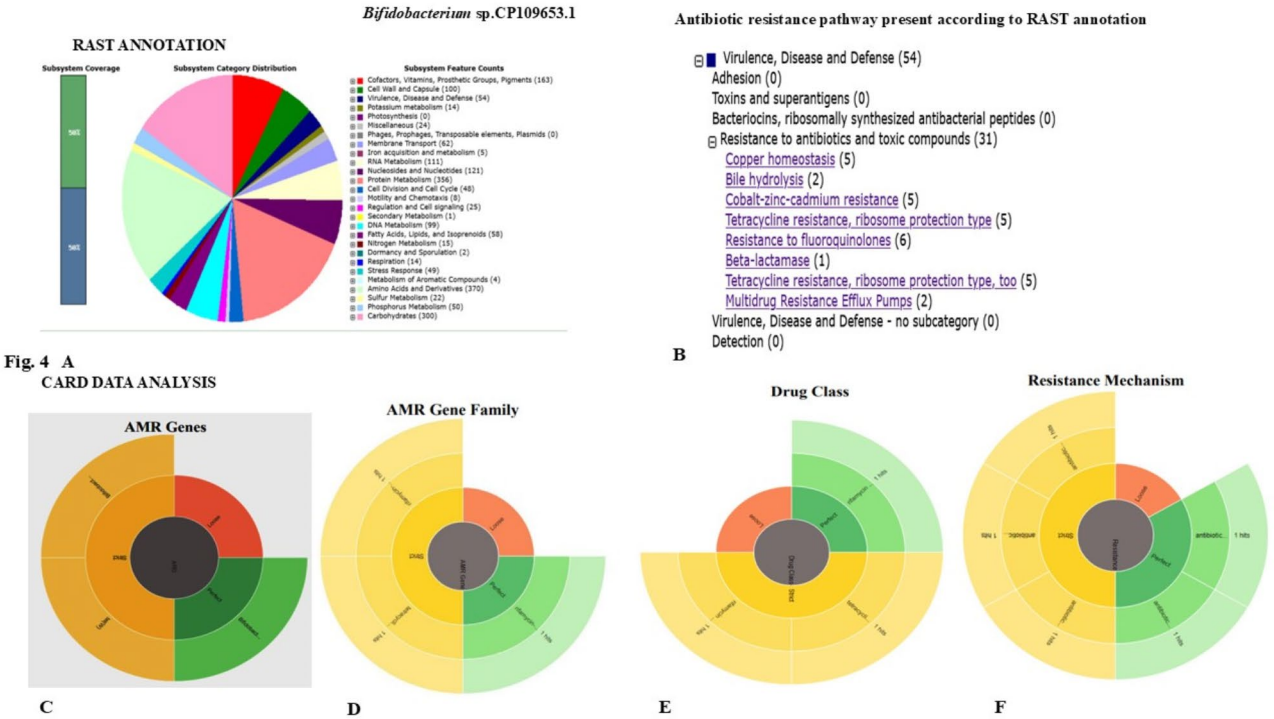

Fig. 4. (**A**) RAST annotation of *B. adolescentis* whole genome sequence showing subsystem coverage, subsystem category distribution, subsystem feature counts. The detailed components of analysis subsystem feature counts are shown. (**B**) RAST annotation analysis showing various antibiotic-resistant pathways present. (**C**) CARD analysis of *B. adolescentis* genome showing AMR genes, gene family, Drug class and resistance mechanisms.

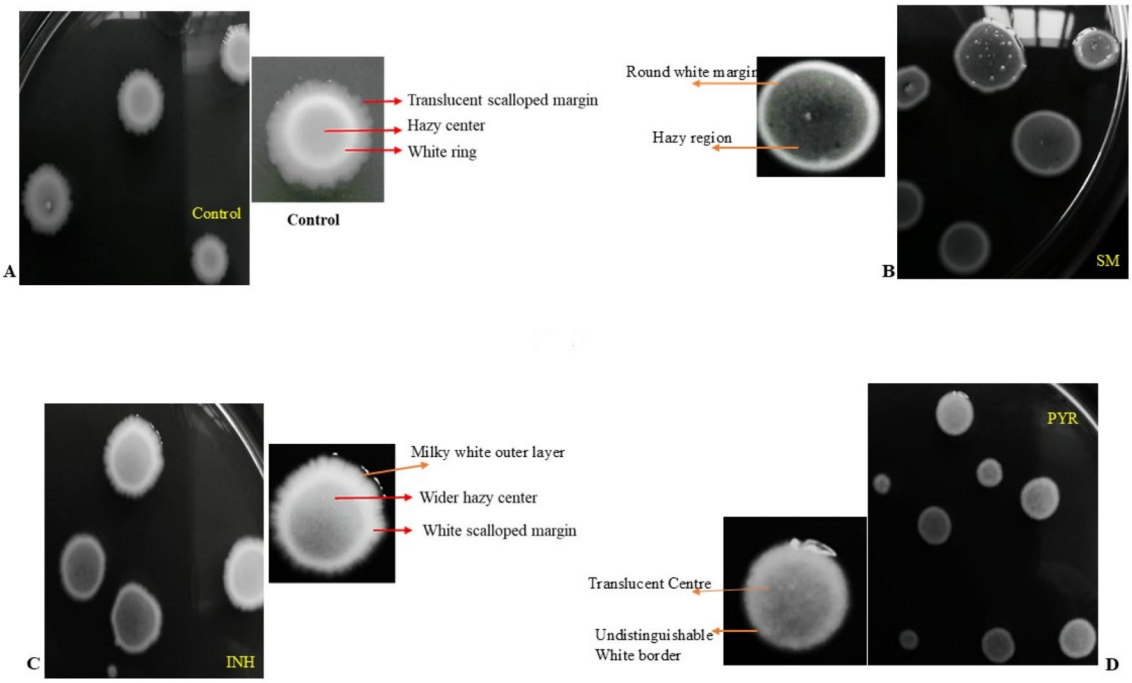

Fig. 5. (**A**–**D**) Surface morphology analysis of various bifidobacteria treated with antitubercular drugs. Procedure followed: *B. adolescentis* was streaked onto MRS agar plate to get an isolated colony. The plate was incubated at 37 °C in an anaerobic gas chamber till to see visual and good growth of colonies. Subsequently, a single isolated colony was inoculated in fresh MRS broth and incubated at 37 °C, 200 rpm for 12 h (now it can grow in aerobic condition). The culture was grown till it reaches 0.5 OD_{600nm}. Now, 10 ml each cell was transferred into fresh sterile tube with respective antitubercular drugs. Here (**A**) is a control containing no antitubercular drugs. (**B**) *B. adolescentis* treated with Isoniazid. (**C**) *B. adolescentis* treated with Streptomycin. (**D**) Pyrazinamide treated *B. adolescentis*. Note: Inset showing various colony morphologies observed.

The first step in drug metabolism is the absorption of the drug. We exposed *Bifidobacterium* to anti-tubercular drugs and found no drug residues, possibly due to rapid degradation. The treated cells showed morphological changes indicating adaptation to the drugs. Our genomic analysis revealed specific resistance factors for rifamycin and tetracycline, which requires further investigation at the proteome level to understand resistance to anti-tubercular drugs. A number of genes and genomic regions found in numerous species, including *Mycobacterium*, are known to contribute to the emergence of resistance to isoniazid (*InhA*), an antibiotic used as the first line of treatment for tuberculosis. *katG* is the other gene cluster associated with resistance. The catalase-peroxidase gene (*katG*) is mutated to reduce the activation of InhA. The way the target drug interacts with InhA is altered by structural or promoter changes in the enoyl acyl carrier protein reductase gene (encoded by *InhA*). An established surrogate marker for *katG* lesions[34–43]. The oxyR-ahpC intergenic region and its mutations are also a cause of resistance (Fig. 6).

However, the latest research shows that not all INH-resistant groups can be identified by studying these regions. The discovery of ketoacyl acyl carrier protein synthase (*kasA*) as a novel target in the mycolic acid biosynthetic pathway has made it possible to identify additional species resistant to isoniazid (INH). These new findings are of crucial importance in the fight against drug-resistant tuberculosis. To determine the presence of *katG* and *kasA*, we screened the entire genome sequence of *B. adolescentis*. We were unable to find *katG* and *kasA* in the genome of *B. adolescentis*.

In 1999, Ann et al. reported polymorphic sites of *kasA* in both resistant and susceptible isolates and their association with antibiotic resistance. Mutations were identified in sixteen resistant isolates, distributed as follows: $^{R}121^{K}$ ($n=1$), $^{G}269^{S}$ ($n=3$), $^{G}312^{S}$ ($n=11$) and $^{G}387^{D}$ ($n=1$). Most of these isolates (13 of 16) had resistance-associated mutations in additional genes[43]. Six of the thirty-two (19%) susceptible strains had the specific polymorphism $^{G}312^{S}$. In the end, they concluded that the *kasA* mutation is not indicative of INH resistance and that testing this target is not important for diagnosis. Therefore, the determination of their resistance cannot be attributed to the mutations in *kasA* alone. According to Li Wan et al. (2020), INH resistance is mostly caused by mutations in the *katG* gene. *InhA*, *ahpC*, *kasA*, *ndh*, *iniABC*, *efpA*, *fadE*, *furA*, Rv1592c and Rv1772 are the second most common causes[44–46]. Li Wan provides additional evidence that INH-resistant isolates have low mutation rates in the coding regions of *inhA and ahpC*, *kasA and efpA*. He goes on to say that further studies on the phenotypic effects of these mutations are needed to confirm that these mutations are associated with INH resistance. We have conducted the same research as the incomplete and deficient *B. adolescentis* genomic research, although all of these studies cast doubt on a link between *kasA* and INH resistance.

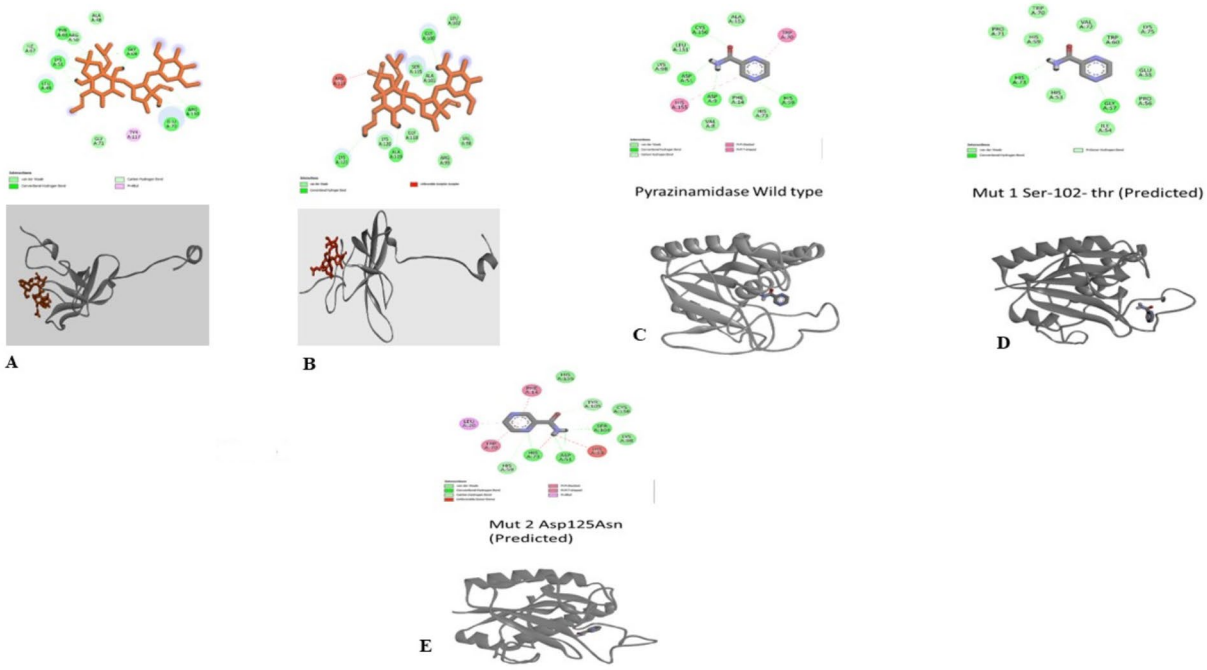

Fig. 6. (**A**–**E**) 3D-Structure Prediction, and Docking studies of Pyrazinamidase and *rpsl*. To determine the homology model of Nicotinamidase/pyrazinamidase, s12 protein and its mutant of *B. adolescentis*, we used canonical amino acid sequence from NCBI (https://www.ncbi.nlm.nih.gov). I-TASSER suite (https://zhanglab.ccmb.med.umich.edu/I-TASSER/), the structure of Nicotinamidase /Pyrazinamidase, s12 protein and its mutants synthesized by *B. adolescentis* was calculated. The model which has highest confidence score was used for structural analysis and docking studies. Pyrazinamide and streptomycin are used as ligand for respective proteins. Docking was performed in AutoDock Tools (ver. 1.5.7) and the complex was visualized and processed using Discovery Studio 2020. (**A**) Represents 3D-structure as well as docking structure of *rpsL* wildtype of *B. adolescentis*, (**B**) *rpsL* mutant $^{K}88^{R}$ 3D-structure and docking structure, (**C**) Pyrazinamidase 3D- and Docking structure, (**D**) Predicted structure of PYR mut $^{S}102^{T}$, (**E**) Predicted structure of PYR mut $^{D}125^{N}$.

Ramifications of the study

B. adolescentis can be considered for antibiotic and probiotic therapy due to its intrinsic resistance to antitubercular drugs and its probiotic properties. According to Wipperman et al. (2017), tuberculosis drug therapy is one of the highest antimicrobial exposures ever experienced by humans. The long-term effects on the stability and composition of the gut microbiome are unknown. The study by Wipperman concludes that TB treatment leads to a significant decline in important commensal bacteria such as *Lactobacillus*, *Bifidobacterium*, *Coprococcus* and *Ruminococcus*, with this phenomenon persisting for at least 1.2 years after treatment. In addition, a significant change in taxonomy was observed, such as a sharp decline in the good bacteria associated with the synthesis of short-chain fatty acids, which are important for intestinal health and general health. In contrast, the administration of probiotics, particularly *Bifidobacterium* spp[47–52]. , in combination with traditional anti-tuberculosis drugs has shown the potential to restore and maintain a healthy microbiome. These therapies have been shown to improve immunological responses.

Materials and methods

Bacterial strains used and their maintenance

All Bifidobacterial strains were obtained from the German culture collection center (DSMZ, Germany). They were grown in De Man, Rogosa, and Sharpe (MRS) Brain Heart Infusion (BHI) or Nutrient Broth Media (NB). Various anti-tubercular drugs, such as rifamycin (RIF), streptomycin (Sm), isoniazid (INH), and pyrazinamide (PYR), were obtained from Hi-Media Laboratories (Mumbai, India). *B. adolescentis* being microaerophilic, at the initial stages of growth, they were first streaked from the glycerol stock to a MRS plate, and they were then incubated in a small anaerobic jar apparatus (with a gas pack containing 3.5 L of polycarbonate, Hi-Media Laboratories, Mumbai, India) at 37 °C for 72 h. After 72 h, small isolated colonies were inoculated into fresh MRS broth in a 15 mL Falcon tube with 10–12 mL of media incubated at 37 °C without shakinguntil an OD_{600} of 2.0 was reached. Glycerol stocks were made with these cultures and stored at -80 °C.

Growth curve studies

The growth curves of the various Bifidobacteria, such as *B. adolescentis* and *B. asteroids*, were studied at 37 °C. The following protocol was strictly followed: A total of 10 mL of freshly prepared MRS broth was cultured at 37 °C without agitation. Then, fresh streaking was impeccably done and single-isolated colonies were introduced into it. Next, 4.0% of the freshly grown cultures were subcultured into 50 mL of MRS medium to start the growth curve at a plate number of 0.01–0.05. The growth curve was closely monitored under the same circumstances. Bacterial samples were periodically taken every 12 h and absorbance was calculated using a precise plate reader scale.

Preparation of anti-tubercular drugs

Three anti-tubercular drugs were considered for the growth curve studies: PYR, INH, and Sm. The miscibility of each drug differs from each other. PYR is dissolved in DMSO (5.0%), INH is soluble in 3.5% ethanol, and SM is soluble in water. Therefore, after dissolving the drug, the growth curves were followed, wherein only DMSO and ethanol were considered as the right controls. In the case of PYR growth curve studies, two controls were considered: (1) a low pH, and (2) 5.0% DMSO.

Analysis of growth pattern in the presence and absence of anti-tubercular drugs

4.0% of the Bifidobacteria cultures were promptly transferred to fresh MRS medium (50 mL), which contained various anti-tubercular drugs. We measured the absorbance at OD_{600} and collected samples every 6 h to analyse the growth curves with and without anti-tubercular medications. We performed each experiment three times, meticulously measuring the absorbance and plotting it against time.

Spot assay

As explained above, 72-hour-grown Bifidobacteria of OD_{600} 1.0 were considered for spot assay. MRS agar plates with and without antibiotics (MIC) were prepared. Subsequently, the resulting 1.0 OD_{600} cells were serially diluted to 10^{-5} in fresh MRS media (900 µL media and 100 µL culture). Serial dilutions were made, and one µL of each dilution was spotted on plates with and without antibiotics. Plates were incubated at 37 °C in an anaerobic gas chamber for 48 h and analysed for growth[53].

Anti-tubercular drug uptake and surface analysis

We followed standard protocols for measuring anti-tubercular drug uptake, such as HPLC. Since this is a very sophisticated and sensitive, it also helps in the estimation of the approximate molecular weight of a substance[54]. Once cells have been exposed to anti-tubercular drugs to understand the surface texture and distinguish rough and smooth strains of Bifidobacteria. The agglutination reactions with acriflavine solution (1/1000) and the capacity to uptake crystal violet[55] were followed. The treated cells were photographed to understand their morphologies.

B. adolescentis adaptability studies

B. adolescentis (0.5–0.8 OD_{600}) was grown in the presence of PYR (1.0 mg/mL), INH (1.0 mg/mL), and Sm (25–100 µg/mL). Every 6.0 h, samples were withdrawn and harvested by centrifugation at 5000 rpm for 20 min. Subsequently, cells were processed by following Bhat et al.'s procedure.

To summarize the process, the cells were collected and washed thoroughly. Next, they were dissolved in a potent organic mixture of methanol, chloroform, and water (12:5:3, 3.0 mL) and subjected to a high temperature treatment of 65 °C for 20 min. The cells were then stored at -20 °C for 12 to 16 h, followed by centrifugation. The unlysed cell debris was promptly removed, and the supernatant was collected and centrifuged at high speed for 15 min. The supernatant was then efficiently dried under a vacuum and the pellet was dispersed in 50 mM, 300 µL of phosphate buffer at pH 7.0. With another round of centrifugation, the organic layer was dried, and the samples were reconstituted in an HPLC buffer on the day of analysis, making them ideally suited for HPLC analysis.

Field emission scanning electron microscopy (FE-SEM) studies

The investigation employed Field Emission Scanning Electron Microscopy (FE-SEM) to thoroughly examine the surface morphology of Bifidobacteria that were treated and untreated with anti-tubercular drugs. The procedures for cultivating and collecting the cells are clearly outlined in the growth curve investigation section. After two phosphate buffer washes, the cell pellets were treated with 2.0% glutaraldehyde and incubated at 4.0 °C for 12–14 h. A gradient of 10–100% ethanol was used to wash the cells, and the sample was ultimately resuspended in absolute alcohol (50–100 µL). An aliquot (~2.0 µL) was placed on a cover slip, dried, and examined under an FE-SEM. Only visually acceptable and compelling photographs magnified by 20,000 times were taken into consideration for further analysis and presentation.

Genomic DNA isolation to understand the modifications at genome level

To extract genomic DNA, GeneJet Genomic DNA Isolation Kit was used. This kit is manufactured by Fermentas, Inc. 830 Harrington Court, Burlington, ON, Canada. The process involved growing a single isolated colony in an anaerobic gas chamber at 37 °C, followed by inoculation into ten millilitres of fresh MRS broth. After that, lysozyme, an enzyme that lyses cell walls, was added to the cells and heated at 37 °C in a Tris-Cl and EDTA buffer with pH 8.0. Later, cells were treated with proteinase K, RNase A, lysis buffer and incubated at room temperature for 10 min. Later, they were centrifuged at 12,000 rpm for 20 min, and the supernatant was loaded into the GeneJet column. The column was washed with wash buffer, and finally, DNA was eluted with Tris. EDTA pH 8.0 before considering further studies, gDNA was electrophoresed to check the quality.

16s rRNA, *rpsL*, *rrs*, and *gidB* gene amplification

The gDNA purified as described above was used as the template for 16 S rRNA amplification using the primers as stated in Table 1. The PCR parameters were: initial denaturation at 95 °C for 5.0 min, followed by 35 cycles of 95 °C for 30s, 56 °C for 45s, and 72 °C for 1.0 min, and a final extension at 72 °C for 5.0 min. DyNAzime II DNA polymerase (Thermo Scientific) was used for the amplification. After completion of PCR, the DNA was analysed through 1.0–1.5% agarose electrophoresis (based on the molecular weight of the amplified fragment). The same template DNA was used for 16 S rRNA, *rpsL*, *rrs*, and *gidB* amplifications.

Particle size analysis to determine bacterial size

As per the previous reports, light scattering technology may be one of the best, cheaper, and most reproducible ways to understand cell diameter, size, and shape. Light-scattering measurements have a crucial advantage over other methods as they require only a minute quantity of sample. Dilute samples are preferred as they aid in simplifying data processing, minimizing multiple scattering events. For the first time, Wyatt et al. reported the use of light scattering technology to identify bacterial cells[56]. Therefore, we followed recent technologies that have been extensively used to understand and measure cell shape and diameter. The procedure begins with the growth of Bifidobacteria in MRS for 72 h at 37 °C in the presence and absence of PYR, INH, and Sm. Subsequently, harvested cells were washed twice with phosphate buffer and re-suspended in fresh phosphate buffer, vortexed to remove the cell clumps, and used for the scattering study. Particle size has been analysed by a Microtrack particle size analyzer (Microtrac SDC; 90–250 VAC; 47–63 Hz, USA). Corresponding chromatograms were collected and analysed.

Catalase foam assay

In Tadayuki Iwase et al. (2013), a simple assay to measure catalase activity was followed. The assay is, in brief, A Simple Assay for Measuring Catalase Activity[57]. We followed this methodology because of its simplicity and because it is a qualitative approach for measuring catalase activity. This study employs commonly available chemicals such as hydrogen peroxide, Triton X-100, and commercial catalase.

Various + ve and -ve controls for the assay, such as *Salmonella typhi* (+ ve, grown in BHI media) *and Lactococcus lactis* (-ve), were considered. *B. adolescentis*, along with the controls, were grown in fresh MRS media (10 mL). Overnight grown 0.5 and 1.5 OD_{600} cells (approximately 10^5–10^7 cells) of 2.0 mL each in transparent test tubes were harvested and washed with phosphate buffer twice. Later, centrifuged to obtain a pellet, 100 µL of Triton X-100 and 100 µL of H_2O_2 (30%) were sequentially added. The reaction mixtures were mixed well and incubated at room temperature for 5–10 min. Upon completion of the reaction, the height of the O^2-forming foam in the reaction tube was measured with a scale. The various tubes with various samples of O^2 foam were photographed. The foam assay kinetics were followed, wherein samples of bacterial cultures were withdrawn at 0, 6, 12, 18, 24, 30, and 36 h. Each sample was processed as explained. The graph was drawn between time and the height of the foam formed, and pictures were taken accordingly.

Catalase gel assay / Zymogram

An established catalase zymogram assay procedure by Magdalena et al. (2018) was employed[58]. Briefly, the process is as follows: The native gels were electrophoretically separated, washed in MQ for ten minutes, incubated in a solution of freshly prepared 0.01% OR 4.0 mM H_2O_2 (made from a 30% stock) for ten minutes, and then rinsed in 100 mL of MQ for thirty minutes. The gels were then incubated in a freshly prepared solution containing 1.0% ferric chloride hexahydrate and 1.0% potassium ferricyanide trihydrate while being gently agitated. One can observe the formation of a set of strong achromatic bands on a green-blue background. To avoid overstaining, immediately the gel was removed from the staining solution and placed in MQ water.

Growth curve studies of *B. adolescentis* in presence and absence of H_2O_2

To understand the ability of *B. adolescentis* to sustain physiological concentrations of H_2O_2, we followed the growth curve in the presence of various concentrations of H_2O_2, such as 1.4 and 6.0 mM. The procedure followed in brief: a fresh streaked plate containing a single isolated colony was inoculated into 10 mL of fresh MRS and was grown at 37 °C without shaking under microaerophilic conditions as stated above. Subsequently, after 72 h of growth, a 1.0% culture was inoculated into fresh MRS broth in the presence of two different concentrations of H_2O_2, as stated above. The OD_{600} at the beginning of the growth curve studies was kept at 0.05; samples were collected at various intervals, and growth was followed for 60 h. Finally, the graph was plotted between OD_{600} and time.

MIC determination

The micro-broth dilution method was followed to determine the MIC of *B. adolescentis* to anti-tubercular drugs such as PYR, INH, and SM[59]. The method followed in brief: *B. adolescentis* was grown as explained above. Once the absorbance value of the cells hit 0.4, they were categorized as being in the mid-exponential growth phase. Following this, the culture was promptly adjusted to a final cell count of 4.0×10^5 CFU/mL to ensure optimal growth and development. 100 µL of bacterial cells were introduced into each well. Subsequently, the highest to the lowest concentration of anti-tubercular drugs were added, making the final volume of the reaction 200 µL. Immediately, serial dilutions were followed that brought down the drug concentration. The reaction mix was mixed well and incubated at 37 °C overnight without shaking. The minimum inhibitory concentration (MIC) was unequivocally determined by the observation of no discernible growth within the well. The MIC was followed for PYR, INH, and Sm for Bifidobacteria three times.

Particle size analysis

After being cultivated in MRS broth for 36 h, *B. adolescentis* was sub-cultured at a 1.0% inoculum level into 15 ml of MRS broth supplemented with various antitubercular drugs. Such as 25 µg/mL, 50 µg/mL, and 100 µg/ml of streptomycin, as well as Pyrazinamide (PYR) dissolved in 100% dimethyl sulfoxide (DMSO) and isoniazid (INH) dissolved in 70% ethanol. In addition, PYR-treated cultures were exposed to low pH levels using acidic MRS media; a control culture that was just grown MRS broth was also included. In order to obtain cell pellets, cultures were centrifuged at 6000 rpm for 15 min using a REMI R-24 centrifuge, after being cultured under microaerophilic conditions for 36 h at 37 °C. Pellets were re-suspended in 1.0 mL of double-distilled water for analysis after being cleaned in autoclaved phosphate-buffered saline (PBS) at pH 7.0. A Microtrac particle size analyzer was used to evaluate the distribution of particle sizes (MICROTRAC SDC; 90-250VAC; 47–63 Hz, USA). Dynamic Light scattering (DLS) was an institutional facility that analyzes particle size ranging 0.8–6500 nm.

Whole genome sequence analysis and AMR prediction

We have employed a variety of bioinformatics tools and databases, including the Comprehensive Antibiotic Resistance Database (CARD), to comprehend the resistance of *Bifidobacteria adolescentis*. CARD[60] was created to record gene sequences carrying multiple antibiotic resistance genes together with pertinent metadata. Resistance gene identifier (RGI) and BLAST are further CARD tools for quick identification and visualisation of antibiotic resistance genes in new, unannotated genomes. Information gathered from systematic reviews for *N. gonorrhoeae* AMR was incorporated in a recent release (3.0.3) of CARD. Kubanov et al. used the RGI web portal from CARD to search for and analyse AMR genetic determinants in genomic sequences of *N. gonorrhoeae* strains[61–63].

Rapid annotation using subsystems technology (RAST)

RAST is another tool used to predict AMR profiles in a given bacterium. *B. adolescentis* whole genome sequence was analysed for the presence of various AMR genes by using RAST. We were mainly interested in looking for the antibiotic-resistance pathways present in the genome.

CARD (comprehensive antibiotic resistance database) data analysis

As said above, this is a tool used to identify AMR genes, AMR gene family, Drug class, and resistant mechanism existing.

Determination of important virulence, disease, and defence related genes

The genome of *Bifidobacterium* was functionally annotated with the NCBI prokaryotic genome annotation pipeline (PGAP) v. 4.7 and rapid annotations using subsystems technology (RAST)[60,62]. Figure 4A–F show the RAST annotation antibiotic resistance pathway present in Bifidobacteria. Further, CARD data analysis shows AMR genes, gene families, drug classes, and the resistant mechanisms involved.

Using the genome functional annotations, the presence of virulence, disease, and defence genes was manually searched and discovered in 54 different categories. Within the category of antibiotic and hazardous chemical resistance, there were thirty-one subcategories. They include beta-lactamase (1), ribosome protection types to (5), tetracycline resistance, bile salt hydrolysis (2), cobalt-zinc-cadmium resistance (5), tetracycline resistance, ribosome protection type (5), resistance to fluoroquinolones (6), and multidrug resistance efflux pumps (2).

3D-structure prediction/homology modelling and docking studies

We utilized the canonical amino acid sequence from NCBI (https://www.ncbi.nlm.nih.gov) to determine the homology model of Nicotinamidase/pyrazinamidase, the S12 protein, and its mutations in *B. adolescentis*. We determined the Nicotinamidase/Pyrazinamidase S12 protein structure and mutations using the I-TASSER suite (https://zhanglab.ccmb.med.umich.edu/I-TASSER/). In the PDB database, we found that nicotinamidase/pyraz inamidase and its mutations were unequivocally similar to 3PL1 (Pyrazinamidase of *Mtb*), whereas s12 protein and its mutants were unmistakably similar to 7BGD (s12 protein of *S. aureus*). The model with the greatest confidence score was utilized for the structural evaluation and docking investigations. Pyrazinamide and streptomycin, two anti-tubercular drugs, were unequivocally used as ligands for their corresponding proteins. Docking was performed in AutoDock Tools (ver. 1.5.7) and the complex was visualized and processed using Discovery Studio 2020.

Data availability

B. adolescentis WGS sequences were submitted to NCBI, and the accession number is GCA_025908335.1 (BioSample: SAMN31249017). Bioproject: PRJNA889585 Bifidobacterium sp. KRGSERBCFTRI. Sample name: Sample1; SRA: SRS15588028.NCBI identification file: CP109653.1URL: https://www.ncbi.nlm.nih.gov/biosample/?term=SAMN31249017.

Received: 7 May 2024; Accepted: 28 October 2024
Published online: 28 November 2024

References

1. World Health Organization. *Anti-tuberculosis Drug Resistance in the World: Fourth Global Report* (World Health Organization, 2008).
2. Wang, Y. et al. The roles of *rpsL*, *rrs*, and *gidB* mutations in predicting streptomycin-resistant drugs used on clinical *Mycobacterium tuberculosis* isolates from Hebei Province, China. *Int. J. Clin. Exp. Pathol.* **12**(7), 2713 (2019).

3. Kiepiela, P., Bishop, K. S., Smith, A. N., Roux, L. & York, D. F. Genomic mutations in the *katG, inhA and aphC* genes are useful for the prediction of isoniazid resistance in Mycobacterium tuberculosis isolates from Kwazulu Natal, South Africa. *Tuber. Lung Dis.* **80**(1), 47–56 (2000).
4. Singh, A., Somvanshi, P. & Grover, A. Pyrazinamide drug resistance in *RpsA* mutant (Δ 438A) of *Mycobacterium tuberculosis*: Dynamics of essential motions and free-energy landscape analysis. *J. Cell. Biochem.* **120**(5), 7386–7402 (2019).
5. Somoskovi, A., Parsons, L. M. & Salfinger, M. The molecular basis of resistance to isoniazid, rifampin, and pyrazinamide in *Mycobacterium tuberculosis*. *Respir. Res.* **2**, 1–5 (2001).
6. Alangaden, G. J. et al. Mechanism of resistance to amikacin and kanamycin in *Mycobacterium tuberculosis*. *Antimicrob. Agents Chemother.* **42**(5), 1295–1297 (1998).
7. Bakuła, Z. et al. Mutations in the embB gene and their association with ethambutol resistance in multidrug-resistant *Mycobacterium tuberculosis* clinical isolates from Poland. *BioMed Res. iInt.* https://doi.org/10.1155/2013/167954 (2013).
8. Allana, S. et al. pncA gene mutations associated with pyrazinamide resistance in drug-resistant tuberculosis, South Africa and Georgia. *Emerg. inf. dis.* **23**(3), 491 (2017).
9. Cuevas-Córdoba, B. et al. (*rrs* and *rpsL* mutations in streptomycin-resistant isolates of *Mycobacterium tuberculosis* from Mexico. *J. Microbiol. Immunol. Inf.* **46**(1), 30–34 (2013).
10. Almuneef, M. et al. *Brucella melitensis* bacteremia in children: Review of 62 cases. *J. Chemother.* **15** (1), 76–80 (2003).
11. Cascio, A. et al. Treatment of human brucellosis with rifampin plus minocycline. *J. Chemother.* **15**(3), 248–252 (2003).
12. Al Shaalan, M. et al. Brucellosis in children: Clinical observations in 115 cases. *Int. J. Inf. Dis.* **6**(3), 182–186 (2002).
13. Moorman, D. R. & Mandell, G. L. Characteristics of rifampin-resistant variants obtained from clinical isolates of *Staphylococcus aureus*. *Antimicrob. Agents Chemother.* **20**(6), 709–713 (1981).
14. Schurig, G. G. et al. Biological properties of RB51; a stable rough strain of *Brucella abortus*. *Vet. Microbiol.* **28**(2), 171–188 (1991).
15. Morishita, T. & Yura, T. Altered nutritional requirements associated with mutations affecting the structures of ribonucleic acid polymerase in *Lactobacillus casei*. *J. Bacteriol.* **125**(2), 416–422 (1976).
16. Dhanashree, L., Raman, P. & Rajagopal, K. *Bifidobacterium adolescentis* is intrinsically resistant to anti tubercular drugs. *Sci. Rep.* **8**, 11897 (2018).
17. Zhang, Y., Wade, M. M., Scorpio, A., Zhang, H. & Sun, Z. Mode of action of pyrazinamide: disruption of *Mycobacterium tuberculosis* membrane transport and energetics by pyrazinoic acid. *J. Antimicrob. Chemothe*. **52** (5), 790–795 (2003).
18. Sheen, P. et al. Effect of pyrazinamidase activity on pyrazinamide resistance in *Mycobacterium tuberculosis*. *Tuberculosis* **89**(2), 109–113 (2009).
19. Zhang, Y., Shi, W., Zhang, W. & Mitchison, D. Mechanisms of pyrazinamide action and resistance. *Microbiol. Spectr.* **2**(4), 10–1128 (2014).
20. Peterson, N. D., Rosen, B. C., Dillon, N. A. & Baughn, A. D. Uncoupling environmental pH and intra-bacterial acidification from pyrazinamide susceptibility in *Mycobacterium tuberculosis*. *Antimicrob. Agents Chemother.* **59**(12), 7320–7326 (2015).
21. Dillon, N. A., Peterson, N. D., Feaga, H. A., Keiler, K. C. & Baughn, A. D. Anti-tubercular activity of pyrazinamide is independent of trans-translation and *RpsA*. *Sci. Rep.* **7**(1), 6135 (2017).
22. Scior, T., Meneses Morales, I., Garcés Eisele, S. J., Domeyer, D. & Laufer, S. Antitubercular isoniazid and drug resistance of *Mycobacterium tuberculosis*—a review. Archiv Der Pharmazie. *Int. J. Pharmaceu Med. Chem.* **335** (11-12), 511–525 (2002).
23. Kim, H. J., Shin, S. I., Lee, S. J., Moon, T. W. & Lee, C. J. Screening and selection of *Bifidobacterium* strains isolated from human feces capable of utilizing resistant starch. *J. Sci. Food Agric.* **98**(15), 5901–5907 (2018).
24. Singh, S., Sankar, M. M. & Gopinath, K. High rate of extensively drug-resistant tuberculosis in Indian AIDS patients. *Aids*. **21**(17), 2345–2347 (2007).
25. Lokesh, D., Rajagopal, K. & Shin, J. H. Multidrug resistant probiotics as an alternative to antibiotic probiotic therapy. *J. Infectiol. Epidemiol.* **2**(4) (2019).
26. Overbeek, R. et al. The SEED and the rapid annotation of microbial genomes using subsystems technology (RAST). *Nucleic Acids Res.* **42**(D1), D206–D214 (2014).
27. Stoffels, K., Mathys, V., Fauville-Dufaux, M., Wintjens, R. & Bifani, P. Systematic analysis of pyrazinamide-resistant spontaneous mutants and clinical isolates of *Mycobacterium tuberculosis*. *Antimicrob. Agents Chemother.* **56**(10), 5186–5193 (2012).
28. Rahman, A. et al. Pyrazinamide susceptibility and pncA mutation profiles of *Mycobacterium tuberculosis* among multidrug-resistant tuberculosis patients in Bangladesh. *Antimicrob. Agents Chemother.* **61**(9), 10–1128 (2017).
29. Cohen, K. A. et al. Evidence for expanding the role of streptomycin in the management of drug-resistant Mycobacterium tuberculosis. *Antimicrob. Agents Chemother.* **64**(9), 10–1128. 2020 (2020).
30. Zuur, M. A. et al. Intermediate susceptibility dose-dependent breakpoints for high-dose rifampin, isoniazid, and pyrazinamide treatment in multidrug-resistant tuberculosis programs. *Clin. Inf. Dis.* **67**(11), 1743–1749 (2018).
31. Hayashi, K. et al. Purification and characterization of oxygen-inducible haem catalase from oxygen-tolerant. *Bifidobacterium Asteroides Microbiol.* **159**(Pt_1), 89–95 (2013).
32. Nair, J., Rouse, D. A., Bai, G. H. & Morris, S. L. The rpsL gene and streptomycin resistance in single and multiple drug-resistant strains of *Mycobacterium tuberculosis*. *Mol. Microbiol.* **10**(3), 521–527 (1993).
33. Huang, G., Pan, H., Zhu, Z. & Li, Q. The complete genome sequence of *Bifidobacterium longum* LTBL16, a potential probiotic strain from healthy centenarians with strong antioxidant activity. *Genomics* **112**(1), 769–773 (2020).
34. Altamirano, M. et al. Mutations in the catalase-peroxidase gene from isoniazid-resistant *Mycobacterium tuberculosis* isolates. *J. Inf. Dis.* **169**(5), 1162–1165 (1994).
35. Deretic, V., Pagán-Ramos, E., Zhang, Y., Dhandayuthapani, S. & Via, L. E. The extreme sensitivity of *Mycobacterium tuberculosis* to the front-line antituberculosis drug isoniazid. *Nat. Biotechnol.* **14**(11), 1557–1561 (1996).
36. Haas, W. H. et al. Molecular analysis of *katG* gene mutations in strains of *Mycobacterium tuberculosis* complex from Africa. *Antimicrob. Agents Chemother.* **41**(7), 1601–1603 (1997).
37. Heym, B., Alzari, P. M., Honore, N. & Cole, S. T. Missense mutations in the catalase-peroxidase gene, *katG*, are associated with isoniazid resistance in *Mycobacterium tuberculosis*. *Mol. Microbiol.* **15**(2), 235–245 (1995).
38. Kapur, V. et al. Y. Rapid *Mycobacterium* species assignment and unambiguous identification of mutations associated with antimicrobial resistance in *Mycobacterium tuberculosis* by automated DNA sequencing. *Arch. Pathol. Lab. Med.* **119** (2), 131–138 (1995).
39. Kelley, C. L., Rouse, D. A. & Morris, S. L. Analysis of ahpC gene mutations in isoniazid-resistant clinical isolates of *Mycobacterium tuberculosis*. *Antimicrob. Agents Chemother.* **41**(9), 2057–2058 (1997).
40. Lee, A. S. G. et al. Lack of clinical significance for the common arginine-to-leucine substitution at Codon 463 of the *katG* Gene in Isoniazid-Resistant *Mycobacterium tuberculosis* in Singapore. *J. Inf. Dis.* **176**(4), 1125–1127 (1997).
41. Marttila, H. J., Soini, H., Huovinen, P. & Viljanen, M. K. katG mutations in isoniazid-resistant *Mycobacterium tuberculosis* isolates recovered from Finnish patients. *Antimicrob. Agents Chemothe*. **40**(9), 2187–2189 (1996).
42. Morris, S. et al. Molecular mechanisms of multiple drug resistance in clinical isolates of *Mycobacterium tuberculosis*. *J. Inf. Dis.* **171**(4), 954–960 (1995).
43. Lee, A. S., Lim, I. H., Tang, L. L., Telenti, A. & Wong, S. Y. Contribution of kasA analysis to detection of isoniazid-resistant *Mycobacterium tuberculosis* in Singapore. *Antimicrob. Agents Chemother.* **43**(8), 2087–2089 (1999).
44. Wan, L. et al. Genomic analysis identifies mutations concerning drug-resistance and Beijing genotype in multidrug-resistant *Mycobacterium tuberculosis* isolated from China. *Front. Microbiol.* **11**, 1444 (2020).

45. Embden, J. D. Characterization of the catalase-peroxidase gene (*katG*) and inhA locus in isoniazid-resistant and-susceptible strains of *Mycobacterium tuberculosis* by automated DNA sequencing: restricted array of mutations associated with drug resistance. *J. Inf. Dis.* **173**(1), 196–202 (1996).
46. Mdluli, K. et al. Inhibition of a *Mycobacterium tuberculosis* β-ketoacyl ACP synthase by isoniazid. *Science*. **280** (5369), 1607–1610 (1998).
47. Wipperman, M. F. et al. Antibiotic treatment for tuberculosis induces a profound dysbiosis of the microbiome that persists long after therapy is completed. *Sci. rep.* **7**(1), 10767 (2017).
48. Unissa, A. N., Subbian, S., Hanna, L. E. & Selvakumar, N. Overview on mechanisms of isoniazid action and resistance in *Mycobacterium tuberculosis*. *Inf. Genet. Evol.* **45**, 474–492 (2016).
49. Maji, A. et al. Gut microbiome contributes to impairment of immunity in pulmonary tuberculosis patients by alteration of butyrate and propionate producers. *Env Microbiol.* **20** (1), 402–419 (2018).
50. Eribo, O. A. et al. The gut microbiome in tuberculosis susceptibility and treatment response: guilty or not guilty? *Cell. Mol. Life Sci.* **77**, 1497–1509 (2020).
51. Namasivayam, S. et al. Longitudinal profiling reveals a persistent intestinal dysbiosis triggered by conventional anti-tuberculosis therapy. *Microbiome*. **5**, 1–17 (2017).
52. Hu, Y. et al. The gut microbiome signatures discriminate healthy from pulmonary tuberculosis patients. *Front. Cell. Inf. Microbiol.* **9**, 90 (2019).
53. Wang, J., Woo, M. & Yan, C. Spot plating assay for the determination of survival and plating efficiency of *Escherichia coli* in sub-MIC levels of antibiotics. *JEMI Methods* **1**(4) (2017).
54. Bhat, J., Narayan, A., Venkatraman, J. & Chatterji, M. LC–MS based assay to measure intracellular compound levels in *Mycobacterium smegmatis*: linking compound levels to cellular potency. *J. Microbiol. Methods* **94**(2), 152–158 (2013).
55. Alton, G. G., Jones, L. M., Angus, R. D. & Verger, J. M. Techniques for the brucellosis laboratory. *Inst. Natl. De La. Recherche Agronomique (INRA)* (1988).
56. Wyatt, P. J. Differential light scattering: A physical method for identifying living bacterial cells. *Appl. Opt.* **7**(10), 1879–1896 (1968).
57. Iwase, T. et al. A simple assay for measuring catalase activity: A visual approach. *Sci. Rep.* **3**, 3081 (2013).
58. Pezzoni, M., Pizarro, R. A. & Costa, C. S. Detection of catalase activity by polyacrylamide gel electrophoresis (PAGE) in cell extracts from Pseudomonas aeruginosa. *Bio-protocol* **8** (11), e2869–e2869 (2018).
59. EUCAST. European Committee for Antimicrobial Susceptibility Testing (EUCAST) ff the European Society of Clinical Microbiology and Infectious diseases (ESCMID): terminology relating to methods for the determination of susceptibility of bacteria to antimicrobial agents. *Clin. Microbiol. Infec.* **9**, 1–7 (2003).
60. Alcock, B. P. et al. CARD 2020: Antibiotic resistome surveillance with the comprehensive antibiotic resistance database. *Nucleic Acids Res.* **48**(D1), D517–D525 (2020).
61. Kubanov, A. A. et al. Whole-genome sequencing of Russian Neisseria gonorrhoeae isolates related to ST 1407 genogroup. *Acta Naturae*. **10**(38), 68–76 (2018).
62. Didelot, X. et al. Genomic analysis and comparison of two gonorrhea outbreaks. *MBio* **7**(3), 10–1128 (2016).
63. Tatusova, T. et al. NCBI prokaryotic genome annotation pipeline. *Nucleic Acids Res.* **44**(14), 6614–6624 (2016).

Acknowledgements
Acknowledgements are due to the Director of CSIR-CFTRI for the facilities provided. DST-SERB and MoFPI are appreciated for funding the project.

Author contributions
KR designed research; KR recruited and managed participants; collected generated data. AN with KR; AN, MVRK, PV, and AC @ KR performed data analyses. KR & AN wrote the paper. All authors read and approved the final manuscript.

Declarations

Competing interests
The authors declare no competing interests.

Acknowledgements
Acknowledgements are due to the Director, CSIR-CFTRI for the facilities provided. DST-SERB, and MoFPI are appreciated for the funding of the project.

Additional information
Correspondence and requests for materials should be addressed to K.R.

Reprints and permissions information is available at www.nature.com/reprints.

Publisher's note Springer Nature remains neutral with regard to jurisdictional claims in published maps and institutional affiliations.